THE ASTROPHYSICAL JOURNAL, 445:999–1016, 1995 June 1

RADIO INTERFEROMETER OBSERVATIONS OF SOLAR WIND TURBULENCE FROM THE ORBIT OF *HELIOS* TO THE SOLAR CORONA

STEVEN R. SPANGLER AND TAKAYUKI SAKURAI
Department of Physics and Astronomy, University of Iowa, Iowa City, IA 52242
Received 1994 July 11; accepted 1994 December 7

ABSTRACT

We report observations of Very Long Baseline Interferometer (VLBI) phase scintillations due to turbulence in the solar wind. The observations were made at 5.00 and 8.42 GHz with the Very Long Baseline Array (VLBA) on three dates in 1991 July and August. We observed the sources 0851+202 and 0735+178 at solar elongations ranging from 2°.66 to 13°.29; the closest approach of the line of sight to the Sun ranged from 10 to 49.8 $R_\odot$. We have also included previously unpublished 5 GHz VLBI phase scintillation measurements from 1989. These measurements probe solar wind density fluctuations on spatial scales from about 200 km to 2000 km. Our measurements are in quite good agreement with the Coles & Harmon model for the radio phase structure function, which was largely determined from observations on both shorter and larger spatial scales. Departures from the Coles & Harmon functions are attributable to day-to-day variations in the solar wind conditions. Phase scintillations at the greatest solar elongations are in very good agreement with extrapolated estimates from direct measurements made with the *Helios* spacecraft at slightly larger heliocentric distances. Thus there is a consistency between the in situ spacecraft and radio remote sensing measurements of density turbulence. All of the VLBI data are consistent with a Kolmogorov spectrum for the density fluctuations, although at the closest elongations there may be excess power at small spatial scales. An advantage of interferometric techniques over other radio propagation measurements is that they provide a measure of the anisotropy of the irregularities. Our observations at closest approach (10 $R_\odot$) show weak evidence for anisotropic, field-aligned density irregularities with an axial ratio of order 2. This degree of anisotropy would appear to be less than that measured at similar solar elongations but on smaller spatial scales by Armstrong and colleagues. Finally, a combination of the radio propagation data and in situ *Helios* measurements is used to determine the heliocentric distance dependence of the normalization coefficient of the density power spectrum, C_N^2. Modeling $C_N^2 \propto (R/R_\odot)^{-\kappa}$, we find $\kappa = 3.72 \pm 0.30$. Subject to a number of assumptions, this result is consistent with the conclusion of D. A. Roberts that turbulence within 0.28 astronomical units adheres to a WKB formula for turbulence amplitude as a function of heliocentric distance.

Nature loves to hide.—Heraclitus

Subject headings: solar wind — Sun: corona — Sun: radio radiation — techniques: interferometric — turbulence

1. INTRODUCTION

Spacecraft observations in the solar wind indicate that it is a turbulent plasma, with fluctuations in all fluid quantities such as magnetic field, plasma flow velocity, and density. Systematic variations in the turbulent characteristics are observed as a function of heliocentric distance, and differences are observed between high-speed streams and regions of slow solar wind flow. Observational studies of this turbulence through spacecraft measurements, and the attendant theory in support of these observations, comprise one of the major areas of space plasma physics. An excellent and recent review of the field is Marsch (1991).

Aside from its interest to basic physics, such magnetohydrodynamic turbulence may play an important role in the formation of the solar wind, and therefore by extension other astrophysical winds. As has been frequently discussed (e.g., Hollweg 1992; Esser et al. 1986), turbulent dynamics may be responsible for accelerating and heating the solar wind to its observed values. It is at this point the above-cited statement of Heraclitus comes particularly to mind. Wave-driven models of the solar wind usually show that the acceleration region, where the turbulent dynamics would be most interesting, is between 5 and 40 $R_\odot$. However, the deepest descent of a spacecraft was *Helios* with a perihelion of 60 $R_\odot$ (0.28 AU). A bona fide test of the wave-driven models obviously requires some experimental information on "hidden" turbulence in the acceleration region.

Radio propagation observations also provide information on turbulence in the solar wind. Since the refractive index of radio waves in a plasma depends directly on the plasma density, propagation through the turbulent solar wind plasma produces a host of scintillation phenomena, known collectively as interplanetary scintillations (IPSs). Reviews of this subject are given in Coles (1978), and more recently by Bourgois (1993). The phenomenon of particular interest to the present paper is interferometer phase scintillation, a random fluctuation in the phase of an interferometer due to interposed turbulence. There are two differences between the in situ measurements of spacecraft such as *Helios* and the remote sensing radio observations considered in this paper. Although obvious, these differences merit emphasis at the outset. First, like most other astronomical observations, scintillations provide information on a path integral of the quantity of interest, whereas spacecraft measure the plasma characteristic at a point. Second, the spacecraft observations measure several plasma parameters of interest, such as the vector magnetic

field, plasma flow velocity, density, and details of the particle distribution functions. In contrast, most scintillation observations are sensitive only to density fluctuations.

This limitation is particularly unfortunate in view of the fact that spacecraft observations indicate that most of the turbulent activity is in the magnetic field and plasma flow velocity. Reasonably accurate comparisons of the observations have been made with Alfvénic turbulence theories, which are totally incompressible. This suggests that much of the time in the solar wind the plasma density is responding to turbulent fluctuations in the magnetic and kinetic energy densities, a notion which has been worked out in considerable formal detail in the pseudosound theory of plasma density fluctuations (Montgomery, Brown, & Matthaeus 1987; Matthaeus et al. 1991). This indicates that the radio astronomical observations are sensitive to a dynamically unimportant tracer of the turbulence, and that a rigorous deduction of turbulent dynamics requires a theoretically sophisticated inversion scheme to deduce the statistics of magnetic and plasma velocity fluctuations from those in density. Such understanding at present does not exist, although some naive attempts will be made in § 4.

The obvious advantage of scintillations is that they may be used to measure turbulence in regions where spacecraft data are not available. This is particularly true of the region interior to the orbit of *Helios*. In this paper we will present Very Long Baseline Interferometry (VLBI) observations of sources whose lines of sight pass inside the orbit of *Helios* and use those observations to obtain characteristics of near-Sun solar wind turbulence. Such observations have obviously been made before, and an extensive literature exists on the subject. In this paper we will make continual reference to the results of Coles & Harmon (e.g., Coles & Harmon 1989; Coles et al. 1991a, b) and Woo (e.g., Woo & Armstrong 1979; Woo & Gazis 1993). The VLBI scintillation results we will present are complementary to those of Coles, Woo, and colleagues. Briefly, VLBI observations are sensitive to density fluctuations on larger spatial scales than those discussed in most of the observations by Coles and colleagues. The results of Woo and colleagues, obtained from measurements of spectral broadening and phase scintillations of a coherent spacecraft transmitter, overlap our range of spatial scales, but the measurable quantity is also dependent on the solar wind velocity, whereas ours is not.

In addition to their relevance to our understanding of the solar wind, interferometric observations of turbulence can also contribute to basic plasma physics. Interferometric observations of sources near the Sun show the scattering to be anisotropic, with the images elongated perpendicular to the interplanetary magnetic field by an amount which is greater than along the field. This anisotropy in the angular broadening was first measured by Hewish (1958) and subsequently studied by other workers (e.g., Blesing & Dennison 1972). The availability of the Very Large Array (VLA) has permitted recent, detailed studies of this phenomenon (Armstrong et al. 1990; Narayan, Anantharamaiah, & Cornwell 1989). Such an effect is a clear indication of anisotropic density irregularities which are stretched out along the magnetic field. Such observations are clearly of importance in determining the nature of turbulence in the inner solar wind. In particular, they support theories that magnetohydrodynamic turbulence itself is two-dimensional and field aligned in cases of low to moderate plasma β (Montgomery & Turner 1981; Zank & Matthaeus 1992).

The outline of this paper is as follows. In § 2, we will discuss the observations. This will involve not only details such as observing times and frequencies, but also how these observations may be used to obtain information on the spectrum and anisotropy of the turbulence. In § 3 the observational results are presented. Section 4 will discuss the implication of the results for our understanding of solar wind turbulence. Of particular interest will be the implications for the evolution of solar wind turbulence from the corona to 50–60 $R_\odot$, i.e., through the putative solar wind acceleration region. Finally, conclusions will be given in § 5.

2. OBSERVATIONAL DETAILS AND THE INFORMATION CONTENT OF THE OBSERVATIONS

This section will be comprised of three subsections. In the first, we describe the physical quantity which we want to extract from the scintillation observations, namely the phase structure function, and discuss how it is related to the turbulence spectrum. The second subsection will deal with the details of the observations, the orientation of the sources with respect to the Sun, etc. Finally, in the third section we describe different ways of processing the data to measure the phase structure function. This will provide an opportunity to display some examples of the data used in our measurements.

2.1. *The Phase Structure Function*

The point of this brief subsection is to write down the basic relationship between observational quantities we can measure with a radio interferometer and the properties of the turbulence. This material is available elsewhere in the literature (Coles 1978; Coles & Harmon 1989; Coles et al. 1991a, b; Sakurai, Spangler, & Armstrong 1992; Armstrong et al. 1990); it is included here for purposes of continuity, and also to define variables which will be used later in the paper.

Scintillation observables are determined by the spatial power spectrum of the plasma density. As is customary, we model this spectrum by

$$P_{\delta n} = C_N^2 q^{-\alpha} , \tag{1}$$

where q is the spatial wavenumber, α is the spectral index, and C_N^2 is the normalization coefficient, which determines the magnitude of the density fluctuations. In this paper, we shall loosely refer to this latter quantity as the "intensity" of the turbulence.

Equation (1) is valid for the case of isotropic turbulence. In actuality, previous radio scattering observations (Armstrong et al. 1990; Narayan et al. 1989 and references therein) show that close to the Sun the density irregularities are anisotropic, in the sense that the irregularities are stretched out along the large-scale magnetic field. This anisotropy is observed to lessen dramatically with increasing heliocentric distance (Armstrong et al. 1990). These anisotropy measurements were from interferometers with much shorter baselines than those considered here, so the size of the irregularities probed was also much smaller. A main goal of the present research is to determine the degree of anisotropy of irregularities with scale sizes of a few hundred to a few thousand kilometers. In any case, we wished to retain the option of considering anisotropic irregularities in our analysis. Anisotropic irregularities may be described by the spatial power spectrum

$$P_{\delta n} = C_N^2[q_x^2 + \eta^{-2}(q_y^2 + q_z^2)]^{-\alpha/2} , \tag{2}$$

where all quantities have been defined above except the anisotropy parameter η. The x direction is taken as that of the large-scale magnetic field.

Scintillation observations are referred to the phase structure function (Coles & Harmon 1989; Coles et al. 1991a, b), defined as

$$D_\phi(s) \equiv \langle [\phi(r) - \phi(r+s)]^2 \rangle , \quad (3)$$

where ϕ is the phase of an electromagnetic wave which has propagated through the turbulent plasma, s is the vector separation between the two points of measurements, and r is an arbitrary reference position. For propagation through a medium which has a density spectrum of the form of equation (1), the phase structure function is given by (Sakurai et al. 1992)

$$D_\phi(s) = 4\pi^2 r_e^2 f(\alpha) \lambda^2 s^{\alpha-2} \int dz' C_N^2(z') , \quad (4)$$

where r_e is the classical electron radius, $f(\alpha)$ is a constant of order unity (Cordes, Weisberg, & Boriakoff 1985) and z' is a coordinate along the line of sight through the turbulent plasma. In the case of observations through irregularities with an anisotropic spectrum given by equation (2), the formula for the structure function is identical to equation (4) except we substitute $(x^2 + \acute{\eta}^2 y^2)^{1/2}$ for s, where x and y are spatial coordinates in the direction of, and perpendicular to, the large-scale magnetic field, respectively. The observed anisotropy $\acute{\eta}$ will generally be less than the true anisotropy η defined in equation (2). For $\acute{\eta}$ to be equal to η, it would be necessary for all magnetic field lines in the scattering volume to be perpendicular to the line of sight. In reality, for the case of radially diverging field lines from the Sun, the angle between the line of sight and the local magnetic field will vary along the line of sight, and $\acute{\eta} < \eta$.

Equation (4) reveals the great utility of IPS observations in deducing the characteristics of density turbulence in a medium. From the measured dependence of D_ϕ on s we can obtain the spectral index α. From the magnitude of D_ϕ we measure the path-integrated value of C_N^2. A line of sight through the inner solar wind will have a point of closest approach to the Sun ("impact parameter") at a distance R_0. Because of the strong radial falloff of plasma density with heliocentric distance, the principal contribution to $\int dz' C_N^2(z')$ will come from the region around closest approach. If we make the simplifying assumption that the turbulence is spherically symmetric, so that C_N^2 is dependent on the radial coordinate r as r^{-4}, then it is easy to show that

$$\int dz'\, C_N^2(z') = \frac{\pi}{2} (C_N^2 R_0) . \quad (5)$$

The justification for the r^{-4} model is the assumption that $C_N^2 \propto n_0^2$ where n_0 is the mean plasma density. As will be discussed in § 4, this assumption is approximately valid in the solar wind.

There are at least two ways of measuring D_ϕ from interferometer data. One way, utilized in Narayan et al. (1989) and Sakurai et al. (1992) is to make a map or image of the turbulently broadened radio source. In this case we have (Sakurai et al. 1992)

$$R(x, y) = \exp [-\tfrac{1}{2} D_\phi(x, y)] , \quad (6)$$

where x, y are defined above, and R is the ratio of the interferometric visibility measured when the source is observed through the turbulent medium, to that when the line of sight does not traverse the inner solar wind, so an interferometer would observe the intrinsic source structure. Thus $R(x, y)$ is the visibility corrected for the intrinsic structure of the source. In the case of a point source, R is equivalent to the visibility of the turbulence-broadened image.

There are a number of shortcomings to measuring the actual broadened image; the amount of scattering must be comparable to or larger than the intrinsic structure of the source, the measured visibility must be corrected for the effects of intrinsic structure, and care must be taken that the visibility is averaged over a time long enough to measure the full effect of the scintillations, but not so long that other interferometric instrumental effects reduce the visibility. A discussion of these effects is given in Sakurai et al. (1992).

An alternative approach, utilized in this study, is to calculate D_ϕ directly from the interferometer phase data. The details of this approach are given in § 2.3.

2.2. *Observations*

Our observations were made on 1991 July 22, August 3, and August 16, using elements of the partially completed Very Long Baseline Array (VLBA). Stations which provided usable data were Kitt Peak, Pietown, Los Alamos, Fort Davis, and North Liberty. Observations were made at 1.66, 4.99, and 8.42 GHz. A combination of low data quality for some scans and excessively heavy scintillations for others compromised the utility of the 1.66 GHz data; in this paper we present selected results for 4.99 GHz and 8.42 GHz only.

The two primary program sources were 0851+202 (OJ 287) and 0735+178. These are both well-known compact extragalactic radio sources which are strong in the centimetric wavelength range. Our VLBI observations provided 5 GHz flux densities of 3.3 and 4.7 Jy for 0851+202 and 0735+178, respectively. Since the sources are of similar flux density, the statistics of their data will be nearly equal from the standpoint of signal-to-noise ratio. In addition to these sources, we also observed the sources 1055+018 and 0552+398, which were far enough from the Sun so that IPS effects were negligible on all 3 days. These sources were observed to monitor array performance and data quality in the absence of IPS.

In Table 1 we list the relevant data on the lines of sight to 0735+178 and 0851+202 on all 3 days of observation. The first column gives the date of the observation, and the second gives the source. Columns (3), (4), and (5) give, respectively, the solar elongation of the source (degrees), R_0 the corresponding impact parameter or distance of closest approach of the line of sight to the Sun (solar radii), and the heliographic latitude of the point of closest approach. The last three quantities were calculated for a representative time within the observing

TABLE 1

SOURCE ORIENTATION INFORMATION

Date (1991) (1)	Source (2)	ϵ (3)	R_0 ($R_\odot$) (4)	Λ (5)
Jul 22	0735+178	7°13	26.7	−26°6
Jul 22	0851+202	11.39	42.7	8.0
Aug 3	0735+178	18.10	67.9	−8.0
Aug 3	0851+202	2.66	10.0	79.9
Aug 16.....	0735+178	30.40	114.0	−4.7
Aug 16.....	0851+202	13.29	49.8	14.0

session. During the July 22 observations, 0735+178 was observed off the west limb of the Sun, while 0851+202 was observed to the east. On August 3, 0851+202 was nearly due north of the Sun, and on August 16 0851+202 was off the western limb of the Sun. As will be shown below, observable phase scintillations were observed for both 0735+178 and 0851+202 on July 22, and 0851+2202 on August 3 and 16. The source 0735+178 was too far from the Sun for reliably detectable scintillations on the latter two dates.

Observations were made with the Mark II VLBI recording system, which has a 1.8 MHz bandpass. Observations consisted of 10 minute scans, and program sources were observed several times during a roughly 12 hr period. Given allowance for telescope move time and initial setup, a typical baseline-scan time series had 8–9 minutes of analyzable data. The number of usable scans at a certain frequency depended on the data quality and scheduling, but was as large as 14. The tapes were correlated with the Mark II VLBI processor at the California Institute of Technology. Data provided were 2 s averages of the raw visibility between the interferometer pairs.

These raw data scans were examined visually and edited. The edited data consisted of raw amplitudes and phases which retained "natural" phase changes due to clock errors, ionosphere, etc. These non-IPS related fringe rates were removed in the usual way by fringe fitting. For all of our scans, a fringe fitting interval of 4 minutes was chosen. This period is much longer than the characteristic timescale of IPS, which is the time for the scintillation pattern to drift across the baseline (Mutel 1975), so we expect that little of the IPS fluctuations were removed from the data, but that systematic visibility variations associated with other effects were removed.

Following this step the data were suitable for analysis. The data at this point consisted of uncalibrated amplitudes and phases, all with a 2 s integration time. Long-term (several minute) systematic phase drifts associated with clock errors, atmospheric changes, etc. had been removed, leaving only phase fluctuations on timescales shorter than 4 minutes. Such variations included interplanetary scintillations, but also radiometer noise, fast tropospheric variations, etc. We did analyze the data by the standard procedures of amplitude calibration followed by hybrid mapping, with the goal of measuring the scintillations via equation (6), as was the case with Sakurai et al. 1992. However, we felt that the better way of measuring D_ϕ was directly through the interferometer phase time series.

These phase time series clearly revealed the presence of IPS, as may be seen in Figure 1. The panel at left shows a phase time series of a source far from the Sun, in which the relatively small variations are presumably due to radiometer noise and atmospheric phase variations. The panel at right shows much larger variations due to IPS. The analysis described in the next subsection was undertaken with data of the form shown in Figure 1.

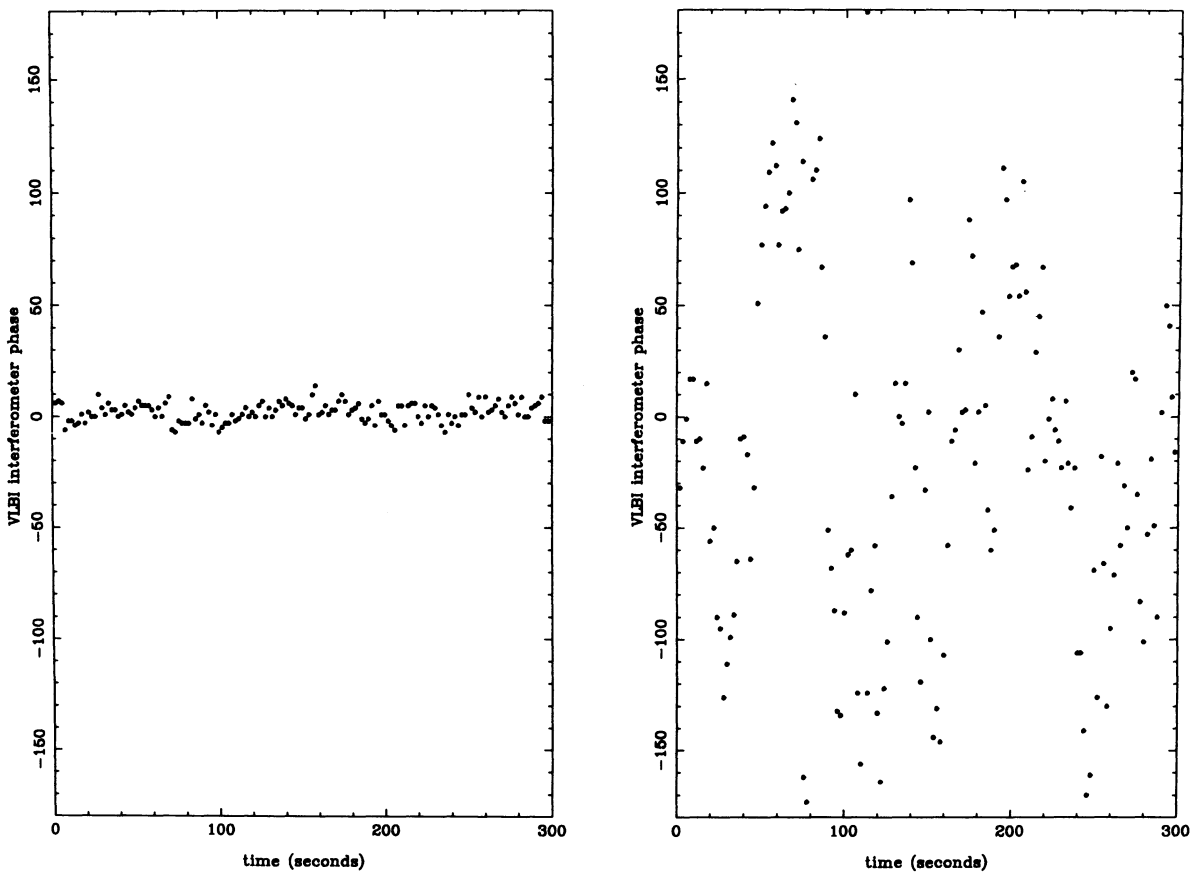

FIG. 1.—Illustration of phase variations for observations of source far from Sun (*left*) and at 10 $R_\odot$ (*right*). The data at left are for 0735+178 on August 16, and are from the Los Alamos–Fort Davis baseline. Phase variations are quite small and due to radiometer noise and possibly unremoved instrumental and atmospheric phase variations. The phase data at right are for 0851+202 on August 3, and are also on the Los Alamos–Fort Davis baseline. The variations are dominated by IPS.

2.3. *Measurement of the Phase Structure Function*

Given a phase time series of the sort shown in Figure 1, the phase structure function (3) may be simply measured as the phase variance σ_ϕ^2 as a function of the baseline length s (or more generally the vector baseline $\mathbf{s}$). However, as will be clearly indicated below, some care must be exercised in choice of the time interval over which σ_ϕ^2 is calculated. There are dangers of erroneous estimation for averaging intervals which are both too short and too long.

If one computes σ_ϕ^2 over too short an interval, say a few seconds, then much of the bona fide scintillation phase power will be filtered out, and the observational estimate of σ_ϕ^2 (and thus D_ϕ) will be biased low. On the other hand, our experience with the data was that too long an averaging time would include fluctuations which do not appear to be part of the IPS process. These extra variations, probably tropospheric phase variations on timescales shorter than the 4 minute fringe fitting time, add to σ_ϕ^2 and thus bias D_ϕ high.

Accordingly, we undertook three methods of measuring σ_ϕ^2. Each of these methods had different advantages, and each allowed the problem of the optimum averaging interval to be addressed in somewhat different ways. We state at the outset that these methods gave measurements of D_ϕ which were in agreement, although the value of σ_ϕ^2 for individual scans varied somewhat depending on the technique. The agreement of the various techniques in calculating D_ϕ gives us confidence in the results presented in this paper.

Phase Temporal Structure Function.—From a phase time series, one can calculate the temporal structure function in a form analogous to equation (3). The structure function rises from the noise floor at the origin to $2\sigma_\phi^2$ on the characteristic timescale of the process. The advantage of this approach is that in the simplest case it directly yields σ_ϕ^2 and shows the timescale on which this occurs.

A good illustration of temporal structure functions is shown in Figure 2, which presents data from 1991 August 16. Shown are temporal structure functions as a function of temporal lag in units of 2 s intervals. The upper three traces show data for 0851 + 202 on the baselines Kitt Peak–Pietown (KP–PT), Los Alamos–Fort Davis (LA–FD), and Los Alamos–North Liberty (LA–NL), which correspond to increasing baseline length. The heavy dashed line at the bottom of the plot is the phase structure function for the source 0552 + 398 on the long LA–NL baseline. The source 0552 + 398 was sufficiently far from the Sun to render IPS phase fluctuations undetectable.

Figure 2 shows that the saturation value of the structure function is larger for all of the 0851 + 202 baselines than for the long baseline for 0552 + 398, and the saturation value increases with increasing baseline length. This fairly clearly shows that IPS phase fluctuations are detectable and measurable, even when the closest approach of the line of sight is 50 $R_\odot$. Equation (4) shows that σ_ϕ^2 should increase with baseline length, and the data in Figure 2 qualitatively show this dependence. These data also clearly show the structure functions rising from the noise floor to a well-defined plateau on a timescale of 10–30 lag units. The lag at which this plateau occurs is defined by the characteristic timescale of the phase scintillations. Clearly, the structure function on the LA–NL baseline would be severely underestimated if one calculated σ_ϕ^2 on 10 s intervals.

The approach to calculating D_ϕ from temporal structure functions was as follows. From plots such as that shown in Figure 2 a value for the plateau of the structure function was chosen. Since the structure function saturates at $2\sigma_\phi^2$, the phase variance was readily measured. This variance was corrected for noise, and equated to D_ϕ on the baseline s characteristic of the scan.

The temporal structure function method, while simple and convenient, presented some difficulties (at least in the form

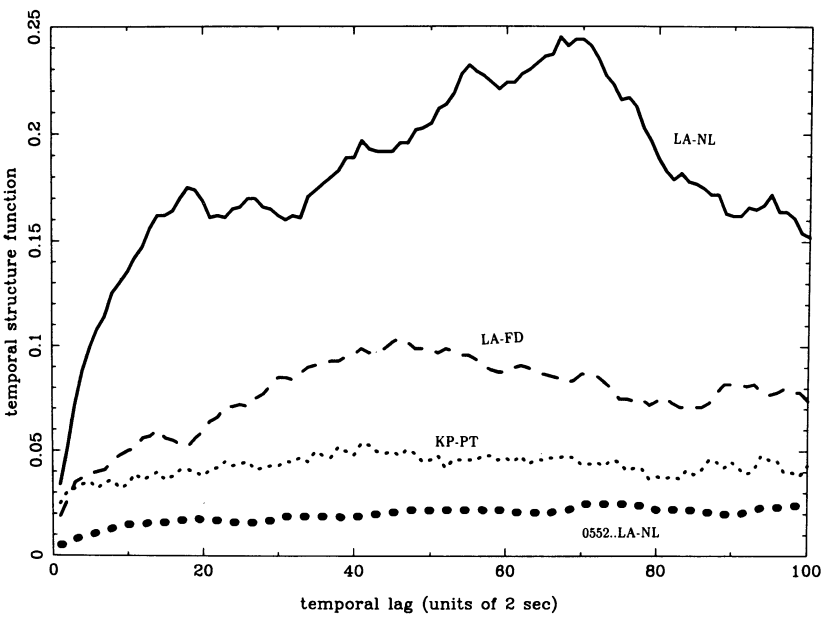

FIG. 2.—Temporal structure functions calculated from phase time series. Plotted is the phase temporal structure function vs. temporal lag in units of 2 s intervals. Upper three traces are for 0851 + 202 on August 16. The baselines KP–PT (*dotted line*), LA–FD (*dashed line*), and LA–NL (*solid line*) are of increasing baseline length, and show larger values for the saturated structure function. The bottom trace (*heavy dotted line*) is for the long (LA–NL) baseline for the source 0552 + 398, which was far from the Sun. The 0552 + 398 data show that phase fluctuations due to residual instrumental and atmospheric effects are small compared with the IPS-induced variations.

implemented by us) which limited its use. First, many structure functions did not show a clearly defined plateau as illustrated in Figure 2. Instead, the structure function would increase to quite large values at large lags. We attributed these cases to unremoved phase variations unrelated to IPS.

The second problem is that for the data set of greatest interest, 0851+202 on August 3, the phase scintillations were too strong to apply the technique, at least in the form we implemented. In the case of a totally random phase time series uniformly distributed on the interval $\pi \rightarrow -\pi$ and delta-correlated in time, the phase temporal structure function has a value of $\pi^2/3$ for all nonzero lags. We found that for 0851+202 on August 3, the measured structure function saturated at $\pi^2/3$ after a few lags. Thus these structure functions could only be used to determine a lower limit to the full, IPS-induced phase variance. Although inadequate, these determinations were nonetheless useful as consistency checks on the results of the techniques described below.

Variances from Filtered Power Spectra.—A way of ameliorating the effects of long timescale, atmospheric, and instrumental phase drifts is to measure the phase variance in the frequency domain. Interplanetary scintillation phase variations occur over a range of frequencies, whereas instrumental and atmospheric phase drifts should be confined to low frequencies. Therefore our second method for determining σ_ϕ^2 was as follows.

1. The phase time series was corrected for phase jumps of 2π. The interferometric visibility does not distinguish between phases of π and $-\pi$ but such jumps obviously cause havoc in a time series. The original phase time series was processed through an algorithm which tested to see if the magnitude of the difference between a phase measurement and its predecessor would be lessened by the introduction of a phase offset of $\pm 2\pi$. If this was the case, a phase offset was added to the phase time series until a subsequent point dictated its removal.

2. The corrected phase time series were Fourier transformed to form a phase power spectrum. These spectra were visually examined and a low-frequency break point chosen which, in many cases, seemed to demarcate the transition between an IPS-dominated spectrum and one in which longer trends were more important. After considerable experience, this low-frequency cutoff was established at 0.020 Hz. The spectra were also examined for a high-frequency cutoff at which the spectra merged with the noise floor. This noise floor was clearly visible for the spectra at the largest solar elongations, but for the observations at smaller R_0 IPS appeared to dominate radiometer noise, even at the Nyquist frequency.

In Figure 3 two specimens of phase power spectra are shown. The left-hand panel shows the spectrum on the LA–NL baseline on August 16. One clearly sees the broadband IPS spectrum merge with the noise floor at a spectral power of about 200. The right panel shows a spectrum from the LA–FD

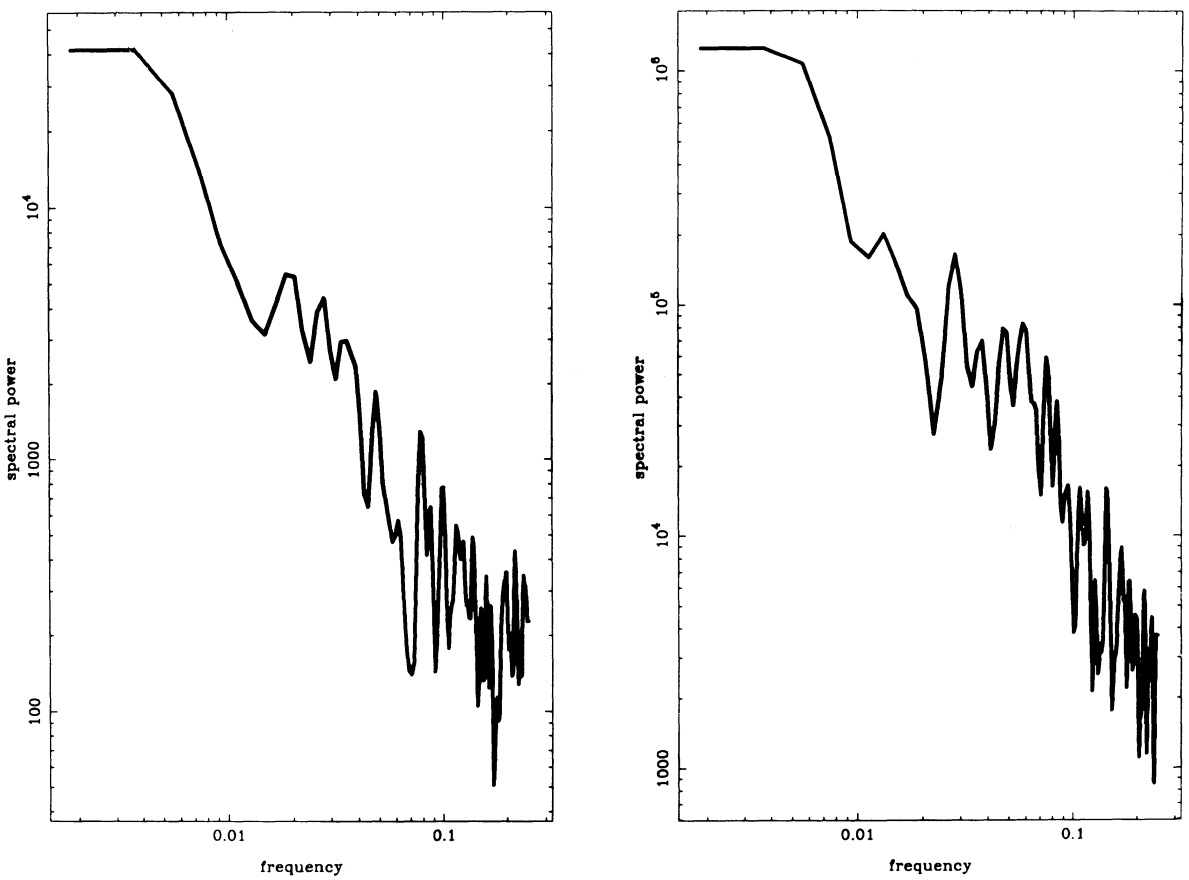

FIG. 3.—Sample phase power spectra. Power spectrum in left-hand panel is from Fort Davis–North Liberty baseline on August 16, when scintillations were relatively weak. The right panel has the spectrum on the Los Alamos–Fort Davis baseline on August 3, the day of closest approach. The great difference in the level of phase spectral power is readily noticeable.

baseline on the day of closest approach, August 3. The spectral power is far greater than the radiometer noise floor at all frequencies.

3. A filtered variance was computed from the power spectrum, with the filtered variance defined as

$$\sigma^2_{\rm filt} \equiv \int_{f1}^{f2} df P(f) , \tag{7}$$

where $f1$ was the lower cutoff frequency (usually 0.020 Hz) and $f2$ was the upper cutoff frequency, which was the either the frequency of the noise floor or the Nyquist frequency when the noise floor could not be discerned.

4. The filtered variance cannot be directly used to measure D_ϕ, since it does not represent the full σ^2_ϕ, but rather only that portion which lies in a frequency range in which IPS is prominent relative to noise and instrumental variations. We therefore corrected the filtered variances by a theoretical factor R_a, so that $\sigma^2_\phi = R_a \sigma^2_{\rm filt}$, where R_a is the ratio of the filtered variance to the total variance which would be measured by a noise and systematic-free interferometer.

For the computation of R_a we used the work of Mutel (1975) who developed a theory for interferometer phase and amplitude scintillations in the presence of plasma turbulence. Mutel (1975) employed the Rytov approximation, which is valid in the case of weak scintillations. The conditions for validity of the Rytov approximation are satisfied for the observations presented in this paper. We used Mutel's equation (3.3.1a) for the theoretical power spectrum $P_{\rm th}(f)$. The value of R_a was then taken simply as $R_a = \int_0^\infty df P_{\rm th}(f) / \int_{f1}^{f2} df P_{\rm th}(f)$.

A few remarks are in order regarding point (4). Mutel's expression for the phase power spectrum $P_{\rm th}(f)$ depends on the solar wind speed, the baseline length, and the baseline orientation with respect to the radial direction, so the resultant value of R_a used to correct our filtered variances depends on these factors as well. For observations of sources far from the Sun, the solar wind speed was estimated from published solar wind velocities as measured by *Pioneer Venus Orbiter*. These measurements say nothing about the solar wind speed close to the Sun, so for the 0851+202 observations on August 3, we used a theoretically motivated value of 200 km s^{-1} for the solar wind speed.

Of the parameters determining the form of the theoretical power spectrum, the strongest dependence is on the baseline length. Nonetheless, for most of the scans processed, the value of R_a was relatively close to 2, and an analysis of the sort we are presenting here could probably be reasonably carried out, omitting precise calculation of $P_{\rm th}$ and simply applying a universal value of $R_a = 2$. The greatest error would be encountered on long baselines and in slow solar wind, where the appropriate value of R_a should be 4 or even slightly larger.

Direct Variance Calculation.—Our third method was to directly calculate the phase variance from the phase time series. This method was undertaken to ensure that the filtered variances calculated from the power spectra were not dominated by unremoved phase jumps. First of all, step (1) from the procedure for calculating the spectrally filtered variance was followed. The jump-corrected phase time series for all baselines and scans considered were then plotted and examined. For each phase time series, portions of the scan were chosen which appeared to be unquestionably free of jumps. For each scan, from one to three such intervals were chosen, varying in duration from perhaps $1\frac{1}{2}$ minutes to several minutes in duration. For each such interval, a linear trend was removed from the phase data and the variance of the trend-removed data calculated. The mean of the variances from the intrascan intervals was calculated, with the provision of excluding anomalous values if there was a sufficient number of intervals.

These variances were not corrected for the finite length of the interval over which the mean was calculated. Since the mean variance was computed from a number of intervals of varying duration, such a correction was not so straightforward as was the case for the filtered power spectrum. Furthermore, the direct variance calculation had the relative virtue of being a quite simple observable, computed without the intercession of a theoretical correction factor.

The data analysis therefore made use of three methods of computing D_ϕ which, although they obviously utilized the same original phase time series, made quite different approaches to extraction of the phase structure function. The agreement between the methods was in general quite satisfactory. Further display of the agreement between the techniques is given in § 3.2 for the 0851+202 data of August 3, for which we had the greatest concern about the possible presence of systematic error.

Error Estimates and Potential Systematic Errors.—Measurement of the phase structure function consists of measurement of the variance of the phase time series. If the variance of a time series is ξ, then the standard deviation of the variance σ_ξ is given by

$$\frac{\sigma_\xi}{\xi} = \sqrt{\frac{2}{N}} , \tag{8}$$

where N is the number of independent measurements.

It is clear from the data presented above, e.g., in Figures 2 and 3, that N is far less than the number of 2 s samples in a scan. Very little of the total variance is realized on timescales of the sample spacing of 2 s. As mentioned above in regard to the temporal structure function, a characteristic lag at which the temporal structure function saturated was 20–40 s. If we take the mean of these values to extract a timescale for independent measurements of 30 s, the appropriate value for N is reduced to 18, and the expected estimation error is 33%. If we instead use 50 s, the inverse of the low-frequency cutoff to the filtered power spectra, as the interval between independent measurements, the estimation error per baseline-scan estimate increases to 43%.

The validity of these estimates is borne out by some of the calculations to be discussed in § 3.2, in which plausible reduced χ^2 values are obtained, provided that $\sigma_\xi/\xi \simeq 0.33$–$0.43$. The significance of the above remarks is that the relatively long correlation time in the VLBI phase time series engenders a significant estimation error for scans of 10 minutes duration.

We next briefly discuss a potential systematic error in the phase structure function measurements when the variation from one 2 s phase measurement to the next is high. This will be a concern when observations are made in strong scattering. Both the filtered variance and direct variance methods of measuring D_ϕ rely on correction of the measured phase time series for jumps of 2π. This was the first enumerated step in the procedures for calculation of D_ϕ from the filtered variance. As noted in the description of this technique, the algorithm seeks to minimize the phase difference between two adjacent measurements. It does this by inserting offsets of $\pm 2\pi$ when war-

ranted. We will refer to this process as reconstituting the true phase time series from the observed one, which is folded on the interval $-\pi \rightarrow \pi$.

As the strength of scattering increases, the mean square difference between adjacent, 2 s phase measurements will increase, and there will be an associated, increasing probability of a "bad call," in which a true, large phase difference is misinterpreted as a jump, and erroneously compensated. Thus, in the case of strong phase scintillations, in which the sample-to-sample phase difference is of order a radian or greater, the reconstituted phase time series will differ from the true one, and in general our methods of measuring the phase variance will yield a different result than would have been the case, had the true (i.e., unfolded) phase time series been available for analysis.

The potential of such an effect was recognized by us and was one of the motivations for utilizing a number of ways of calculating the phase variance from the data. It also served as an impetus for examining both 6 and 3.4 cm data for the observations of $0851+202$ at the time of minimum solar elongation, when such concerns are most relevant. During the review of this paper, the referee requested a quantitative exploration and discussion of this issue. The investigation described below was therefore undertaken.

We assume that the difference between two adjacent phase measurements ϕ_1, ϕ_2 can be described by a Gaussian probability distribution with $\sigma^2 \equiv \langle(\phi_1 - \phi_2)^2\rangle$. The algorithm which tests for insertion of phase offsets of $\pm 2\pi$ will not encounter difficulties as long as $\sigma \ll 1$ radians, but as $\sigma \rightarrow 1$ radian, there will be "bad calls" by the algorithm, in which a phase offset is inserted to compensate a true, large-phase fluctuation, as well as possibly cases in which large fluctuations obscure the necessity of inserting a phase offset.

It may be shown that the probability of a bad call for a single pair of phase measurements is $P_{er}(\sigma) = [1 - A_G(\pi, 0, \sigma)]$, where A_G is an integral of a Gaussian distribution defined by Bevington (1969). The probability of a bad call occurring in a scan is the aforementioned probability multiplied by the number of phase measurements in the time series. The appropriate value of σ is obtained directly from the dot product structure function described above, $\sigma^2 = D_1$, where D_1 is the phase temporal structure function at unit lag. For the case of the structure functions shown in Figure 2, the value of D_1 is sufficiently small that the probability of encountering a bad call in a 10 minute scan is negligible. However, for the source $0851+202$ on the day of closest approach, D_1 for the 5 GHz data ranged from a mimimum of 0.8 radian^2 to highest values of order 1.8 radian^2. Representative values for most of the baseline-scan combinations were of order 1.5 radian^2. The values were smaller for the 8.4 GHz data.

For the 5 GHz data at closest approach, the expected number of bad calls in a typical scan ranged from $\simeq 0.1$ for the scans with the lowest value of D_1 to $\simeq 5$ for the highest. For the median scans with $D_1 \simeq 1.5$ radian^2, the expected number of bad calls from the above expression was about 2.5.

The effect of these "bad calls" on the derived phase variances, and thus D_ϕ values, was explored via a Monte Carlo approach. Synthetic phase time series were generated in the following manner. The random phase time series was generated in the frequency domain as $\tilde{\phi}(f) = [P(f)/2]^{1/2}(A + \imath B)$, where $P(f)$ is the desired phase power spectrum, and A and B are Gaussian distributed random numbers with zero mean and unit standard deviation. A purely real phase time series in the time domain was ensured by stipulating $\tilde{\phi}(-f) = \tilde{\phi}^*(f)$. For $P(f)$ we chose the previously cited expression of Mutel (1975), evaluated for actual baselines and (u, v)-plane loci encountered in our observations. A second set of simulations was undertaken in which a $f^{-5/3}$ power-law was chosen for $P(f)$ and a less sophisticated scheme for generating the random time series was utilized. The justification for using the latter phase power spectrum is that it often gave a reasonable representation of the entire measured phase power spectrum, including low-frequency components which may not be due to interplanetary scintillations. In either case, the normalization coefficient of the power spectrum was adjusted to reproduce the measured values of D_1.

The output of the phase time series simulation could be chosen in one of two formats. The first was the "true" simulated time series, given simply by the Fourier transform of $\tilde{\phi}(f)$, and corresponding to the measurement made by an ideal, omniscient interferometer. In the second format the phase data were folded onto the interval $-\pi \rightarrow \pi$. This format corresponded to the actual interferometer phase measurements from our experiments. For each simulation, a phase time series in each format was generated and processed through the same set of programs used to analyze the real VLBI data. A comparison of the phase variances emergent from the two formats then allowed us to inspect the effect of the bad calls.

The results of many simulated phase time series, spanning the relevant range of the important parameter D_1, are as follows. First, the total variance of the time series was affected in a way which was dependent on the form of the $P(f)$ chosen. However, this result merely reflects the fact that the presence of bad calls will cause the reconstituted time series to depart from the true one. This fact was recognized during the initial data reduction process and was the impetus for employing several methods for measuring the phase variance, and more importantly, for utilizing techniques which employed some form of filtering to excise the effect of bad calls and other non-scintillation sources of phase fluctuations. The effect of the bad calls on filtered quantities such as the filtered variance was vastly smaller. The parameter used to quantify the effect of the bad calls on a given realization was the ratio of the filtered variance (eq. [7]) for the folded and reconstituted phase time series to that for the true simulated time series. The lowest value for any of our realizations was 0.75 for this parameter, and in some realizations it exceeded unity. Typically, for a set of statistically identical realizations the filtered variance for the folded and reconstituted time series was less than that of the true time series by 10% to (at most) 20%, and in some cases the agreement was even closer. The error thus introduced by this process is smaller than the estimation error associated with a D_ϕ measurement, and also smaller than the error associated with the choice of the filtered variance correction parameter R_a, which depends on the unknown solar wind speed in the scattering volume. Furthermore, the precise magnitude of the effect is probably dependent on the form of the phase power spectrum $P(f)$, determined by contributions from IPS, tropospheric effects, and the fringe fitting process.

An abbreviated examination was made of the effect, if any, of bad calls on D_ϕ measurements obtained from the direct variance measurements. Here the effect of bad calls is militated against through the subjective process of visually choosing data segments which appear to be free of phase jumps. These investigations indicated that the direct variance measurements on the simulated phase time series were in good agreement

with those emergent from the filtered variance technique, and thus not subject to large systematic error. The third of our methods, use of the phase temporal structure function, was immune to phase jumps associated with folding on the interval $-\pi \rightarrow \pi$.

In summary, while a more profound and extensive study of the phase reconstitution process and its effect on VLBI phase scintillations would be very desirable, we see no indication that the D_ϕ values reported in this paper are subject to serious systematic error from the folding and reconstitution process.

3. OBSERVATIONAL RESULTS

In this section we present the results of our phase structure function measurements. Two primary issues will be discussed and are each the subject of a subsection, the dependence of the phase structure function on solar elongation and a detailed discussion of the observations of August 3.

3.1. *Solar Elongation Dependence of Phase Structure Function*

Reliable phase scintillations were detected from both 0735+178 and 0851+202 on July 22, and from 0851+202 on August 3 and August 16. This gives us information on the phase structure function D_ϕ for a range of values of R_0 from 10 to 50 $R_\odot$.

The greatest amount of data is available for the close encounter observation of August 3; for this observation the largest number of baseline-scan data sets were analyzed, in part because an effort was made to measure the degree of anisotropy of the scattering (§ 3.2 below). For the remaining dates and sources, unacceptable data quality or excessively weak scintillations on short baselines reduced the number of scans analyzed.

The results are shown in Figure 4. Shown are the phase structure function measurements as a function of baseline length s. The phase structure functions have been scaled to a fiducial wavelength of 12.6 cm, which is the reference wavelength chosen by Coles & Harmon (1989) and Coles et al. (1991). As may be seen in equation (4), D_ϕ values at different wavelengths are directly proportional to the square of the ratio of the observing wavelengths.

Different symbols in Figure 4 distinguish the observations made at different solar elongations. For all observations other then 0851+202 on August 3, the structure functions shown were calculated from the filtered power spectra of 5 GHz data. For 0851+202 on August 3, the data shown are a subset of the different measurement techniques. A full discussion of the 0851+202 data on this day is given in the next subsection. The solid lines represent the Coles-Harmon interplanetary phase structure function for impact parameters R_0 of 10, 20, and 50 $R_\odot$. These lines are taken directly from Figure 3 of Coles & Harmon (1989).

Figure 4 shows that our phase scintillation measurements are in quite good agreement with the Coles & Harmon model. In particular, the August 16 data with $R_0 = 50\ R_\odot$ and the August 3 data at $10\ R_\odot$ are almost perfectly represented by this model. The agreement of the 0851+202 observations for July 22 are probably adequate. In contrast, the July 22 data for 0735+178, of which there are many measurements, seem significantly higher than the Coles-Harmon model would predict. There is independent support for the presence of enhanced turbulence along this line of sight on 1991 July 22. W. A. Coles (private communication) was making spaced receiver observations of 0735+178 on the day of our observations as well as the day after. Coles reports that the IPS-inferred solar wind velocity on July 22 was 615 ± 15 km s^{-1}, while on July 23 it was a typical low-speed solar wind value of 425 ± 20 km s^{-1}. Such a pronounced change in the solar wind speed on a timescale of a day is somewhat unusual and suggests that the high-speed wind was probably a transient which would be expected to result in enhanced solar wind turbulence. It seems plausible to attribute our elevated scattering measurements to this transient-associated turbulence.

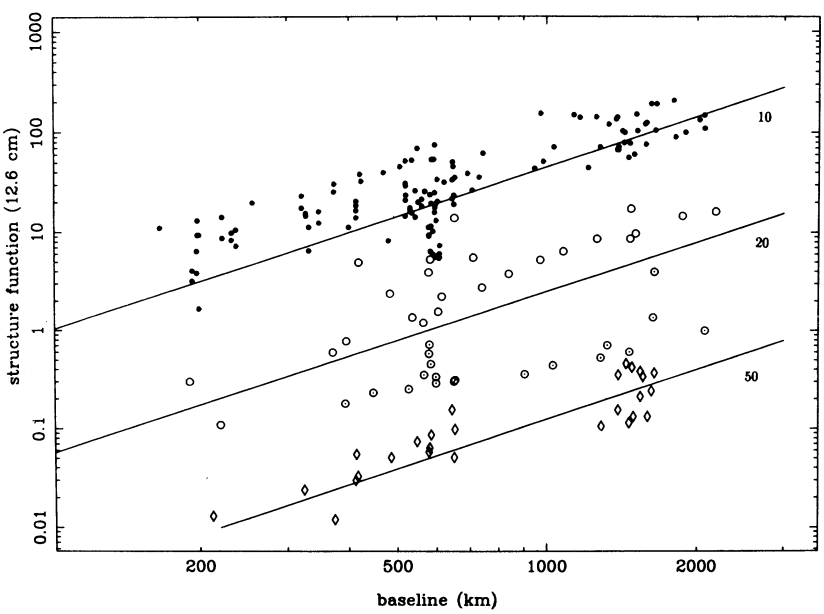

FIG. 4.—Solar elongation dependence of interplanetary phase structure function as deduced from VLBI observations. Shown is the phase structure function $D_\phi(s)$, scaled to a wavelength of 12.6 cm, as a function of baseline s. Observations are as follows. 0851+202 on Aug 3, $R_0 = 10\ R_\odot$, *filled circle*; 0735+178 on July 22, $R_0 = 26.7\ R_\odot$, *open circle*; 0851+202 on July 22, $R_0 = 42.7\ R_\odot$, *dotted circle*; 0851+202 on August 16, $R_0 = 49.8\ R_\odot$, *diamond*. The solid lines represent the Coles-Harmon model for the interplanetary phase structure function at impact parameters of 10, 20, and 50 $R_\odot$.

An important scientific result to be drawn from Figure 4 is its support for a Kolmogorov spectrum of density fluctuations on spatial scales corresponding to the baselines, i.e., 200–2000 km. The lines drawn on Figure 4 all correspond to the Kolmogorov case of $\alpha = 11/3$. The data for all solar elongations are in reasonable to very good agreement with this value for α. The enhancement of spectral power on scales characteristic of the ion inertial length noted by Coles & Harmon (1989) is for the most part confined to smaller spatial scales than those we are measuring, and we have not attempted to represent it in the lines drawn in Figure 4.

The data shown in Figure 4 may be used, with the help of equations (4) and (5), to calculate the dependence of C_N^2 on heliocentric distance. Equations (4) and (5) may be rewritten in the following convenient form:

$$C_N^2 = 1.56 \times 10^{15} D_\phi R_0^{-1} s_{\rm km}^{-5/3} , \quad (9)$$

where D_ϕ is the 12.6 cm phase structure function, R_0 is in units of solar radii, and $s_{\rm km}$ is the baseline length in kilometers. Equation (9) is valid for a Kolmogorov spectrum, and its units are $m^{-20/3}$.

For each of the data sets, a number of ways of least-squares fitting and manual fitting of structure functions to the data in Figure 4 were made. From formal error calculations and the internal agreement of these fits, we obtained a mean value of the phase structure function at the fiducial baseline length of 2000 km, and an estimate of the error of this value. Equation (9) was then used to obtain the value of C_N^2 at the impact parameter R_0. The results are given in Table 2.

In addition to the measurements reported in this paper, we also include other structure function measurements made in 1989 and presented in Sakurai (1993). These data are taken from the same observations reported in Sakurai et al. (1992), but the numbers given in Table 2 were obtained from direct processing of the phase times series in an identical manner as described in § 3. The phase structure functions from which these measurements of C_N^2 were obtained showed excellent adherence to a Kolmogorov spectrum. In addition, we list values of C_N^2 inferred from in situ measurements of density fluctuations by the *Helios* spacecraft (Marsch & Tu 1990). A discussion of this very interesting matter is deferred until § 4.1.

The data from Table 2 are plotted in Figure 5. The solid line is discussed further in § 4; it represents a power-law dependence of C_N^2 on heliocentric distance with a power-law index of -3.72. Figure 5 is presented as a single dependence of C_N^2 on heliocentric distance, with no consideration of heliographic latitude. Bourgois & Coles (1992) have shown that there is indeed a heliographic latitude dependence, but *only for conditions of solar minimum*, at which time the scattering over the solar poles is less than that in the ecliptic plane. At times of solar maximum Bourgois & Coles (1992) find that the strength of scattering is independent of heliographic latitude, and dependent only on the heliocentric impact parameter. The observations reported here were made in 1991, when the Sun was in a prolonged maximum state, so it would appear reasonable to assume circularly symmetric scattering. If this were not the case, the data point corresponding to measurements at 10 $R_\odot$ should be revised upward, which would lead to a steeper power-law dependence of C_N^2 on R. The observations of Sakurai (1993) were made in 1989, and solar maximum conditions should apply. The in situ measurements of Marsch & Tu (1990) were made in the ecliptic plane, and the aforementioned remarks are not pertinent.

3.2. *Observations of 0851+202 on 1991 August 3*

The data set of greatest interest in this project consists of measurements of 0851+202 on August 3, for which we are probing plasma turbulence at 10 $R_\odot$. This is of interest both because this part of space is so remote from the regions of the solar wind where in situ measurements can provide us with guidance, and also because both theoretical models and observational results (Esser et al. 1986; Coles et al. 1991b) indicate that this is well within the acceleration phase of the solar wind. Information on such turbulence is therefore of the greatest interest to models of wave-driven solar wind.

Large numbers of phase structure function measurements were made from both the 5 GHz and 8.4 GHz data, utilizing the filtered variance and direct variance measurements. In addition, phase temporal structure functions were calculated for a subset of the scan-baseline combinations, but, as mentioned in § 2, for these observations the structure functions were usually saturated at $\pi^2/3$. The number of phase time series analyzed per frequency and method of analysis ranged from about 50 to 70.

The resultant structure function is shown in Figure 6. Plotted is the 12.6 cm phase structure function versus baseline length. Estimates emergent from different frequencies and with different computation and analysis techniques are distinguished with different symbols. A number of remarks can be made about the data shown in Figure 6. First, the D_ϕ measurements from both frequencies and techniques are in excellent agreement with the Coles & Harmon (1989) structure function, indicated by the solid line. There may be some indication of a slight excess at short baselines (200–500 km). Second, the D_ϕ measurements utilizing the direct variance calculation at 8.4 GHz lie somewhat below those calculated from the filtered variances. We believe this is due to the omission of the correction (referred to as R_a in § 2) for partial sampling of the variance due to finite interval effects. The theory of phase scintillations (Mutel 1975) indicates that this effect will be most

TABLE 2

C_N^2 VERSUS SOLAR ELONGATION

R_0 ($R_\odot$)	C_N^2 ($m^{-20/3}$)	δC_N^2 ($m^{-20/3}$)	Reference
10.0.....	3.47×10^{10}	1.37×10^{10}	This paper: 0851+202, 1991 Aug 3
18.0.....	2.61×10^{9}	1.89×10^{9}	Sakurai 1993
26.7.....	2.74×10^{9}	0.90×10^{9}	This paper: 0735+178, 1991 Jul 22
35.0.....	1.32×10^{8}	0.80×10^{8}	Sakurai 1993
42.7.....	1.72×10^{8}	0.57×10^{8}	This paper: 0851+202, 1991 Jul 22
49.8.....	3.92×10^{7}	1.96×10^{7}	This paper: 0851+202, 1991 August 16
62.1.....	3.72×10^{5}	1.00×10^{5}	*Helios*: Marsch & Tu 1990
67.8.....	1.31×10^{8}	0.50×10^{8}	*Helios*: Marsch & Tu 1990
72.1.....	8.31×10^{6}	3.00×10^{6}	*Helios*: Marsch & Tu 1990

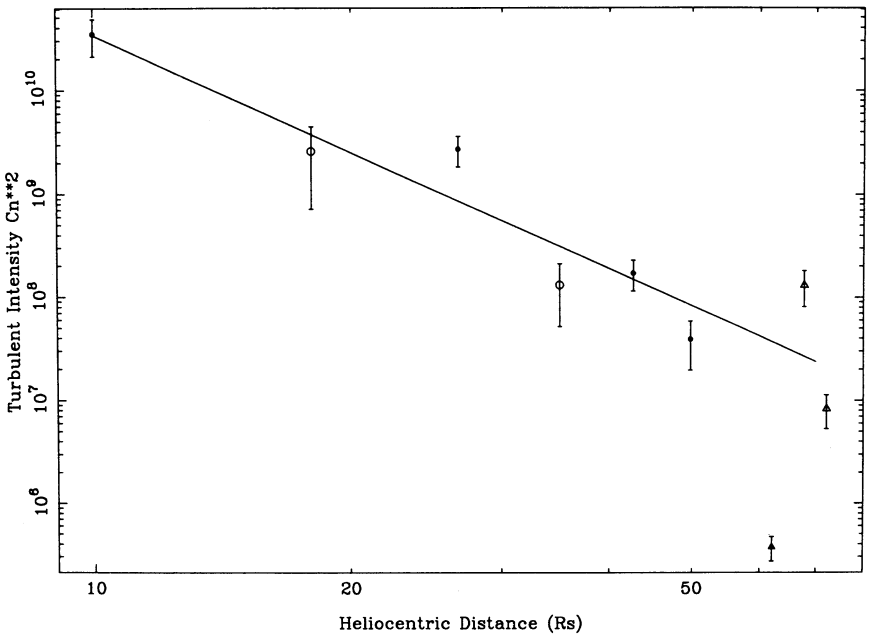

FIG. 5.—Dependence of turbulent intensity C_N^2 on heliocentric distance. Data are as follows: Observations from this paper, *filled circles*; observations from Sakurai 1993, *open circles*; values deduced from *Helios* spacecraft measurements in slow solar wind conditions, *triangles*; and by the *Helios* spacecraft in high-speed solar wind, *filled triangles*. The solid line represents a least-squares fit to a portion of the data, and represents a power dependence of C_N^2 on heliocentric distance.

pronounced for long baselines and slow solar wind speeds. The R_a factors applied to the filtered variances for these baselines typically ranged from 4 to 5; application of such upward correction factors would clearly bring these estimates into good agreement with the other estimates. As is, these measurements serve as good estimates of a lower bound to D_ϕ. However, since we believe the optimum estimation of D_ϕ involves application of the R_a correction, the 8.4 GHz direct variance estimates are not utilized in the remainder of our analysis.

Anisotropy of Scattering.—Figure 6 clearly reveals a factor of several dispersion in the values of D_ϕ for a single value of the baseline. Although we believe much, if not most of this dispersion is due to the large estimation errors in our measurements of D_ϕ, as discussed at the end of § 2, anisotropy of the scattering also would produce increased dispersion. Accordingly we fit the data which comprised Figure 6 with a modified form of equation (4) which took into account the possibility of anisotropic scattering, as discussed in the paragraph following

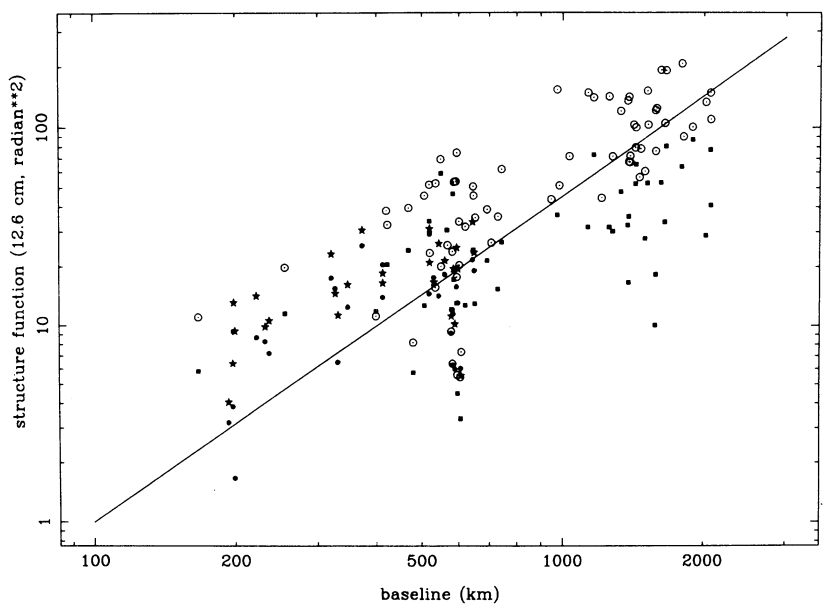

FIG. 6.—Phase structure function D_ϕ at 12.6 cm as a function of baseline length for 0851+202 on 1991 August 3. Each data point represents the result from a phase time series of a given scan-baseline combination. Different symbols indicate different frequencies or methods of phase variance calculation. *Stars*: filtered variances from 5 GHz data; *filled circles*: direct variance at 5 GHz; *dotted circles*: filtered variance at 8.4 GHz; *filled squares*: direct variance at 8.4 GHz. Plotted line represents the Coles and Harmon (1989) structure function for 10 $R_\odot$.

equation (4). Instead of the baseline length s being the relevant parameter, we fit for a "rotundate baseline" $(x'^2 + \dot{\eta}^2 y'^2)^{1/2}$. The coordinates x' and y' are defined in a frame which has been rotated by an angle θ from the radial direction, and $\dot{\eta}$ is the axial ratio of the scattering. In the case of scattering by irregularities which are elongated along the interplanetary magnetic field, θ will be zero and $\dot{\eta} > 1$. In the case of isotropic scattering, $\dot{\eta} = 1$ and θ is arbitrary. The fitting procedure assumed $\alpha = 11/3$. The least-squares fit analysis was undertaken for three data sets; filtered variance with the 5 GHz data, direct variance with the 5 GHz data, and filtered variance with the 8.4 GHz data.

In all three cases, fitting of equation (4) to the data with a rotundate baseline produced a smaller reduced χ^2 than did a fit with the normal baseline s. Furthermore, the three data sets gave consistent values for $\dot{\eta}$ and θ. The value of θ is poorly constrained. Least-squares fits on all three data sets consistently find a χ^2 minimum for $\cos\theta \simeq 0.96$. This is of interest because it indicates magnetic field-aligned irregularities. However, values of $\cos\theta \geq 0.80$ produced a formal χ^2 probability of occurrence greater than 5%, and thus are acceptable.

The anisotropy parameter $\dot{\eta}$ is better constrained. All three sets of data give a least-squares fit with $\dot{\eta} \simeq 2.0$; an anisotropy parameter less than 1.40 can be excluded at the 5% level, and total isotropy excluded with much higher confidence. The net effect of these calculations is that the data favor anisotropic scattering, due to magnetic field aligned irregularities, with an axial ratio of $\simeq 2.0 \pm 0.5$. The anisotropic scattering produces a statistically significant improvement in χ^2 over isotropic scattering, although admittedly not by a spectacular amount.

A simple visual way of seeing the case for anisotropy is to compare plots of D_ϕ versus s and the best-fit rotundate baseline. As discussed in Armstrong et al. (1990), if anisotropy is present the dispersion of points in a plot of D_ϕ versus s will be greater than when the proper rotundate baseline is used. Such a plot is shown in Figure 7 for the 5 GHz, direct variance data. The left-hand panel shows D_ϕ plotted versus baseline, the right-hand panel shows D_ϕ versus a rotundate baseline in which $\cos\theta \simeq 1.0$ and $\dot{\eta} = 2.0$. The dispersion of data points is clearly reduced for the right-hand panel. Similar plots for the 5 GHz and 8.4 GHz filtered variances show a similar effect, although not quite as visually pronounced.

The aforementioned calculations and Figure 7 represent the case for anisotropy of scattering, and thus of the plasma irregularities at 10 $R_\odot$. These results, which pertain to density irregularities with scale sizes of 200–2000 km, can be compared with those of Armstrong et al. (1990), for scales sizes of several kilometers to 35 km. From Figure 5 of Armstrong et al. (1990), we see that the observed axial ratio of scattering for VLA baselines was $\simeq 5$ for an impact parameter of 10 $R_\odot$. This is higher than the anisotropies reported above, and the difference is probably significant in that higher anisotropies would have been easier for us to detect, and produced even greater dispersion of the D_ϕ values than we measure.

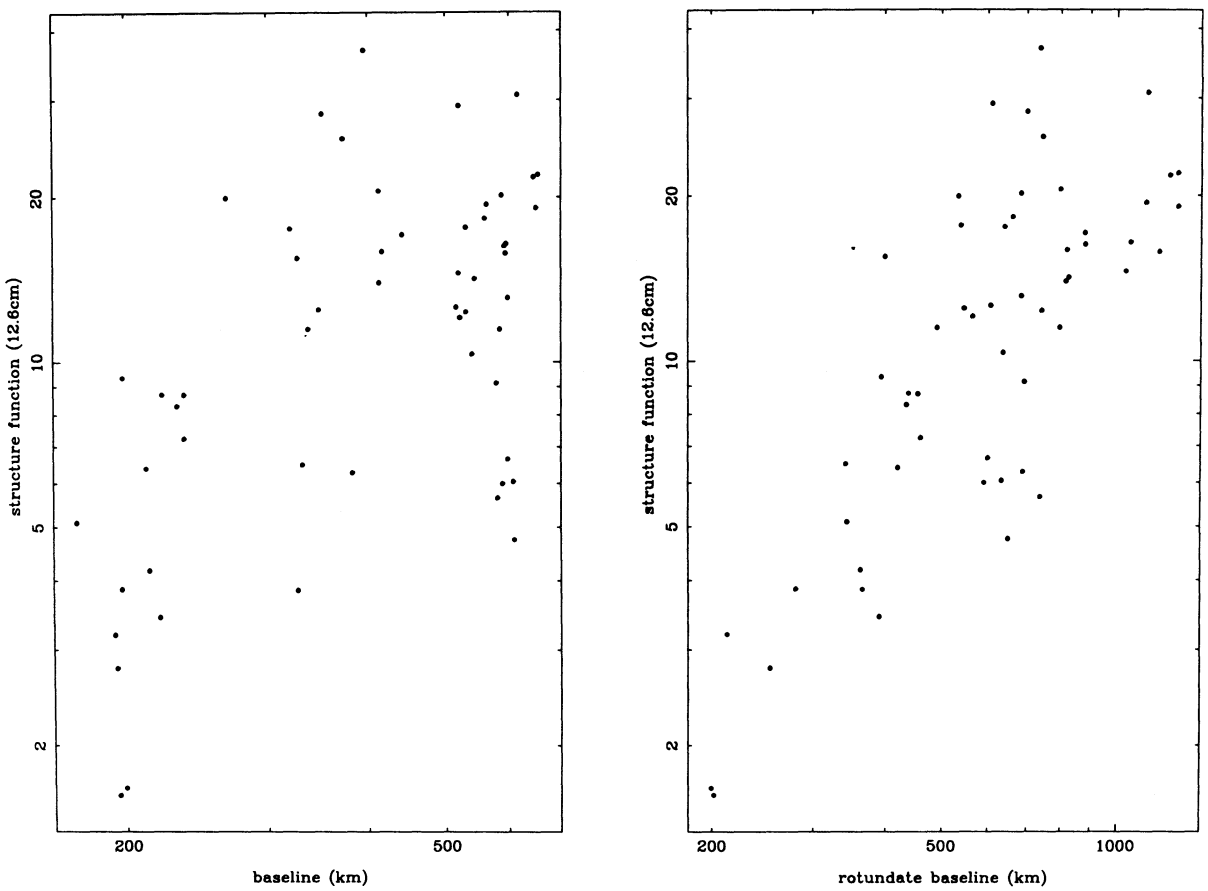

FIG. 7.—Evidence for anisotropy of scattering for 0851 + 202 on 1991 August 3. *Left panel*: Measured values of D_ϕ vs. baseline s for the 5 GHz direct variance data set. *Right panel*: Same D_ϕ measurements plotted against rotundate baseline with a scattering axial ratio of 2.0.

Further interpretation of these results is probably premature until a comparison can be made between VLA and VLBA anisotropy measurements made at the same time. Such an investigation is in progress.

With the above indication that anisotropic scattering is present, we can present a revised version of Figure 6 which takes into account the anisotropy. Such a plot is presented in Figure 8, which shows D_ϕ versus rotundate baseline. Different symbols differentiate ways of calculating D_ϕ according to frequency or method of computing σ_ϕ^2. The rotundate baseline has been calculated with $\cos\theta \simeq 1.0$ and $\dot{\eta} = 2.0$. Again, the dispersion of the points is clearly reduced relative to Figure 6, supporting the evidence for anisotropic scattering. The solid line again represents the Coles & Harmon structure function. Since the increased dispersion due to anisotropic scattering has been presumably removed from Figure 8, the remaining scatter should be due to estimation error, as described in § 2. Therefore the data were binned in intervals in rotundate baseline and averaged. The averaged data are shown in Figure 9. This figure presents our best representation of the scattering structure function at 10 $R_\odot$.

The fact that the measurements of D_ϕ in Figures 8 and 9 lie slightly below (i.e., factor of 2) the Coles-Harmon model is not of significance. We took this model by scaling the curves from Figure 3 of Coles & Harmon (1989). This figure did not distinguish components of the baseline parallel to and perpendicular to the large-scale magnetic field, and thus can be considered a mean of D_ϕ measured in the two orthogonal directions with respect to the field.

The data in Figures 8 and 9 give a slight indication that the power-law index for the dependence of D_ϕ on rotundate baseline, determined for all the data, may be slightly flatter than Kolmogorov. A simple way of realizing this is to have a Kolmogorov spectrum for all scales, with enhanced density fluctuations at the smallest scales of a couple of hundred kilometers. The interesting feature of the density spectrum deduced by Coles & Harmon (1989) is, of course, exactly such an enhancement at short scales. Coles & Harmon (1989) identify the scale of this feature with the ion inertial length, which is of the order of 10 km at 10 $R_\odot$, far shorter than our baselines. Figure 3 of Coles & Harmon (1989) and several plots in Coles et al. (1991a, b) show that for baselines of order 100 km there is an initial indication of a departure from the pure Kolmogorov structure function to a more complex function including the enhancement at the ion inertial scale. Thus although it does not seem likely that this feature should be highly evident in our structure function measurements, it is possible that some trace is detectable on the shortest baselines.

4. DISCUSSION AND INTERPRETATION OF THE OBSERVATIONS

In this section we discuss some of the inferences which can be drawn about solar wind turbulence from the observations presented in § 3.

4.1. *Comparison with Spacecraft Measurements*

Our observations include measurements with impact parameters as large as 50 $R_\odot$. Such heliocentric distances are only slightly less than the perihelion of the *Helios* spacecraft, a fact which invites comparison of the two types of measurement. Previous comparisons of IPS and in situ measurements have been made, but they generally refer to different heliocentric distances, and quite different irregularity scale sizes. IPS intensity scintillations at metric or decimetric wavelengths can be measured for impact parameters greater than 0.30 AU, but are sensitive to irregularities of scale size much smaller than those considered here. Furthermore, such measurements are probably influenced by the spectral enhancement at the ion-inertial scale, which would further confound comparisons with spacecraft measurement. The VLBI measurements here are mainly or totally determined by the Kolmogorov portion

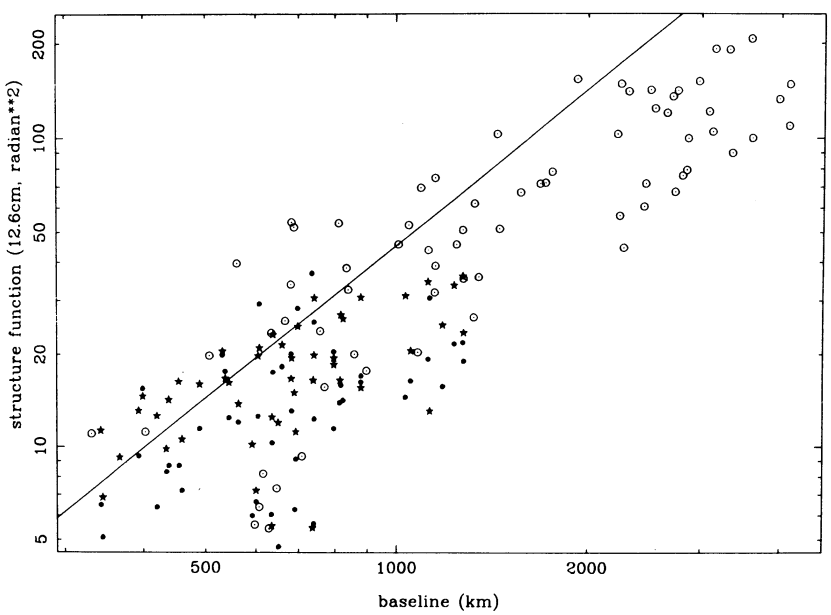

FIG. 8.—Measurement of D_ϕ vs. rotundate baseline. All measurements from 5 GHz direct variance, and 5 and 8.4 GHz filtered variance have been included, and are differentiated by the same symbols as in Fig. 6. The rotundate baseline assumes that the axial ratio of the scattering $\dot{\eta}$ is 2.0, and that the major axis of the anisotropic irregularities responsible for the scattering is approximately aligned with the radial direction. The solid line represents the Coles-Harmon model for the scattering structure function at 10 $R_\odot$.

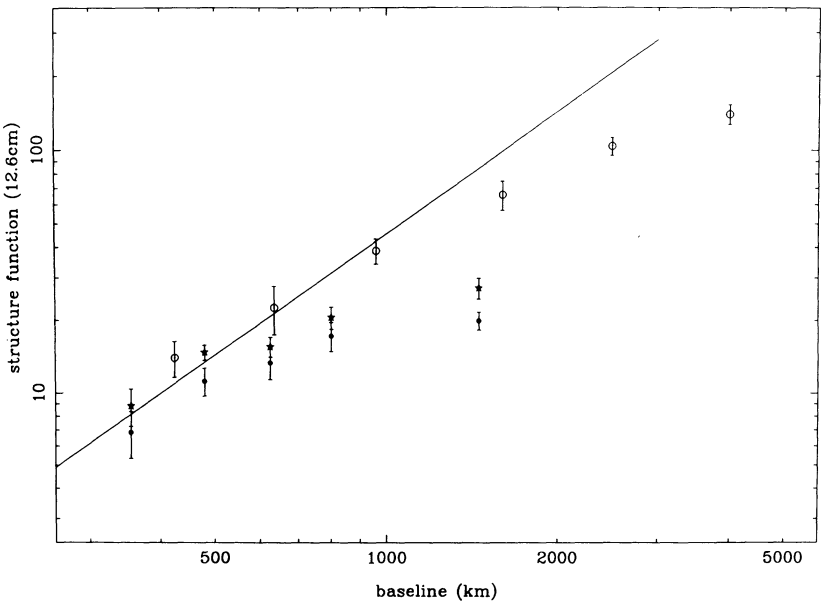

FIG. 9.—Same as Fig. 8, except data have been averaged in selected intervals in rotundate baseline

of the density spectrum, and are much closer to the spatial scales directly measured by spacecraft than are those measured via intensity scintillations. For example, for a solar wind speed of 400 km s^{-1}, the irregularities responsible for fluctuations with a frequency in the spacecraft frame of 2×10^{-3} Hz have a scale $\simeq 3.2 \times 10^4$ km. The VLBI measurements reported here are sensitive to scales of 200–2000 km. Although smaller than the scales directly measured in situ, VLBI is much closer to the relevant scales than are intensity scintillation measurements, which probe scales of order kilometers to a couple tens of kilometers.

A detailed study of the density fluctuations measured by the *Helios* spacecraft at perihelion was presented in Marsch & Tu (1990). We now make a comparison of our data with theirs, cognizant of the fact that these measurements were made 15 yr prior to ours, and during solar minimum. Marsch & Tu present their data in terms of temporal power spectra. Spatial variations are seen as temporal variations in the spacecraft frame because of solar wind convection of the turbulence past the spacecraft. In this frozen turbulence approximation, a spectral feature seen in the temporal power spectrum at frequency f corresponds to a spatial wavenumber $q_x = 2\pi f/V_{sw}$ where V_{sw} is the solar wind speed and q_x is the spatial wavenumber in the radial direction.

In their Figure 1, Marsch & Tu (1990) display temporal power spectra measured by *Helios*. The spectra are of normalized density fluctuations $\delta n/n_0$, but enough information is provided to obtain the temporal power spectra of the density fluctuations $P_{\delta n}(f)$. This figure clearly illustrates one of the main theses of their paper, that the form of the power spectrum depends on whether one is in the high-speed or low-speed solar wind. In the low-speed solar wind, the density spectrum is Kolmogorov, $P_{\delta n}(f) = C_f^2 f^{-5/3}$ for all frequencies. This expression also defines the power spectrum normalization constant C_f^2 for later reference. In high-speed solar wind, there is also a Kolmogorov portion of the spectrum, but Marsch & Tu report a flattening of the power spectra at the highest frequencies before their Nyquist frequency.

Now consider the case for radio wave scintillation. We start with the three-dimensional, isotropic form of the power spectrum, equation (1). This spectrum can be used to deduce the "reduced" power spectrum $P_1(q_x)$ which would be measured by Fourier transforming density measurements along a one-dimensional slice through the turbulent medium. This is obtained by integrating equation (1) over q_y and q_z. The result is

$$P_1(q_x) = \frac{\pi C_N^2}{(\alpha/2 - 1)} q_x^{-(\alpha - 2)} . \tag{10}$$

The correspondence between equation (1) and the temporal power spectra published by Marsch & Tu can be established by noting that $P_1(q_x)dq_x = P_{\delta n}(f)df$ and using the frozen turbulence relation for the connection between f and q_x. Equation (10) gives the following value for C_N^2 which is implied by the power spectra for the case of Kolmogorov turbulence ($\alpha = 11/3$),

$$C_N^2 = (2\pi)^{2/3} \frac{5}{6\pi} V_{sw}^{-2/3} C_f^2 . \tag{11}$$

Equation (11) has been used with the data from Figure 1 of Marsch & Tu (1990) to obtain values of C_N^2 for spectrum "b" at a heliocentric distance of 72.1 $R_\odot$, spectrum "c" at 67.8 $R_\odot$, and spectrum "e" at 62.1 $R_\odot$. The results are given in Table 1 and plotted along with our measurements in Figure 5; the errors listed are totally arbitrary and were not in the paper of Marsch & Tu (1990). We have arbitrarily set them to be about one-third of the mean values. Spectra "b" and "c" were from slow-speed solar wind conditions and are indicated in Figure 5 as open triangles. Spectrum "e" was recorded in high-speed solar wind and is plotted as a solid triangle.

Figure 5 then yields a quite interesting result. The radio scintillation data and the Helios in situ measures show quite good correspondence, provided that regions of slow solar wind dominate the integral of C_N^2 along the line of sight. The reason for this is quite simple and can be appreciated by examination of the figures in Marsch & Tu (1990). The normalized spectra

of fast and slow solar wind are approximately the same, but slow-speed regions are much denser. The density fluctuations δn are therefore much larger and have a bigger effect on radio waves. The value of C_N^2 obtained from the measurements of Marsch & Tu (1990) for a high-speed stream is far below the value obtained from the scintillation measurements.

The results of Figure 5 then suggest that regions of slow-speed solar wind dominate the IPS observations presented here. In using the term dominate, we do not imply that IPS is solely sensitive to turbulence in slow-speed regions. Previous investigations (Kojima et al. 1992; Rickett & Coles 1991 and references therein), using intensity scintillations at much lower frequencies than considered here, have mapped out the heliographic latitude and longitude dependence of the solar wind speed, as well as its dependence on the solar cycle. It is clear from these works that scintillations from high-speed streams are detected.

There are a number of plausible reconciliations of our result, that IPS-inferred C_N^2 values are close to those of slow-speed solar wind, and so much larger than the corresponding values for high-speed streams, with published reports of detectable scintillations from turbulence in high-speed streams. First, even though low-frequency intensity scintillations detect a signature of high-speed streams, the published data leave open the possibility that there is a large, if not dominant contribution from denser regions of slow solar wind. Support for this contention may be found in Rickett & Coles (1991) where it is noted that IPS-inferred solar wind speeds in high-speed streams generally underestimate in situ spacecraft measurements. This is most readily explained via a contribution to the observables from slower and denser regions of the solar wind. This contention receives further support from Ananthakrishnan, Coles, & Kaufman (1980) who showed that enhanced 74.8 MHz scintillation indices could be associated with dense regions of interaction between high-speed streams and slow solar wind.

A second point, and the one which we consider the most likely explanation, is the solar cycle dependence of the solar wind structure. Rickett & Coles (1991) note that at solar maximum IPS inferred velocities tend to be uniformly low over all heliographic latitudes, and coronal densities become more symmetric. Although the remarks of Rickett were primarily concerned with heliographic latitude variations, similar conclusions probably pertain to longitudinal variations. Thus, even for low-frequency intensity scintillations, it appears that observations near solar maximum are most heavily determined by slow solar wind regions.

The third and final point we make in our scheme for internal consistency in the various IPS measurements is to note the result of Kojima et al. (1992) that even at solar minimum, slow solar wind is more prevalent in the volume of space internal to 0.3 AU than it is in the region from 0.3 to 1.0 AU. This point may be appreciated by examination of Figures 1 and 3 of Kojima et al. (1992). One would therefore expect that radio lines of sight passing closer to the Sun than 0.3 AU, as is the case for all of the IPS observations presented in Table 2, would encounter more regions of slow, dense solar wind than would be indicated from in situ spacecraft observations at heliocentric distances of 0.3 to 1.0 AU.

In summary, the above remarks corroborate our contention that although IPS may be used to measure scintillations from high-speed streams, measurements of the strength of scattering on lines of sight through the inner solar wind (impact parameter $\leq 50\ R_\odot$), particularly at times of solar maximum, are likely to be dominated by slow, dense solar wind flows.

Before leaving this subsection, it is interesting to entertain an alternative explanation for the results of Figure 5. The interferometer phase scintillations reported here measure the intensity of density fluctuations on spatial scales of 200–2000 km. The measurements of Marsch & Tu (1990) are of density fluctuations on much larger scales. The results of Figure 5 indicate that a Kolmogorov fit to the spacecraft spectra in high-speed streams, extrapolated to scale sizes of 200–2000 km, predicts less intense density fluctuations that are indicated by our observations. However, as noted above, the high-speed stream spectra of Marsch & Tu (1990) are not pure Kolmogorov spectra, but rather show a spectral flattening on the shortest spatial scales. Taken at face value, these spectra have more density spectral power on spatial scales of 200–2000 km than a pure Kolmogorov power-law. The published high-speed stream spectra would have less of a discrepancy with IPS-deduced values of C_N^2 and would lessen or remove the above arguments for a dominant role of slow speed solar wind in determining IPS measurements.

However, the prior suggestion must also contend with the fact that our IPS observations yield not only the level of the density fluctuations, but also the spatial power spectrum. Our experimental results, as well as those of our colleagues (e.g., Coles & Harmon 1989; Coles et al. 1991a, b; Woo & Armstrong 1979) indicate that the spatial power spectrum on scales of 100–several thousand kilometers is Kolmogorov, or nearly so. If turbulence in high-speed streams makes a significant contribution to IPS observables, and the flattening on short spatial scales reported by Marsch & Tu (1990) is a major spectral feature, the density power spectrum in high-speed streams must be a composite. At large scales greater than 10^5 km the spectrum would be Kolmogorov, have a transition to a flat portion on scales $\sim 10^5$ km, and finally recover a Kolmogorov spectrum on scales probed by IPS. It is not clear what physical processes could produce such a composite spectrum.

4.2. *The Evolution of Hydromagnetic Turbulence inside the Orbit of Helios*

Let us not concur casually about
the most important of matters...

Heraclitus

As discussed in the introduction of this paper, one of the more interesting issues in the sudy of solar wind turbulence is whether it is capable of heating and accelerating the solar wind. The viability of wave-driven theories depends on a quantity which in principle is measurable, the energy density of hydromagnetic waves and turbulence close to the Sun. One of the more important contributions in this area has been the study of Roberts (1989). Roberts (1989) used *Helios* data to analyze the evolution of the normalized magnetic field fluctuation $\delta B/B_0$ as a function of heliocentric distance from 0.3 to 0.9 AU. He found that this amplitude adhered to a WKB prediction for the wave amplitude as a function of heliocentric distance. The WKB formula may be written as

$$\frac{\langle(\delta B)^2\rangle}{\langle(\delta B_0)^2\rangle} = \left(\frac{\rho}{\rho_0}\right)^{3/2} \frac{(1 + V_{A0}/V_{sw0})^2}{(1 + V_A/V_{sw})^2} . \quad (12)$$

In this equation ρ, V_A, V_{sw} represent the plasma density, Alfvén speed, and solar wind speed, respectively, at a given

point in space. A subscript 0 denotes these quantities at a reference level, by convention taken to be the solar wind Alfvénic point at which $V_A = V_{sw}$. For standard solar wind models, equation (12) simplifies to (Roberts 1989)

$$\frac{\langle(\delta B)^2\rangle}{\langle(\delta B_0)^2\rangle} = \frac{\mu^{3/2}}{(1+\sqrt{\mu})^2}, \tag{13}$$

where $\mu \equiv \rho/\rho_0$. These formulas may then be used to calculate the wave energy density and flux from the perihelion of *Helios* all the way to the Alfvénic point in the solar wind. The main point of Robert's argument is that when one uses equations (12) or (13) to extrapolate the observed MHD wave flux at 0.3 AU back to the corona, there is insufficient flux to accelerate the solar wind.

Although Roberts's paper is clearly and tightly reasoned, one could have two reservations. First, there is a sceptical unease about extrapolating MHD wave fluxes over the range 60–10 $R_\odot$ with an allegedly known theoretical scaling formula. Second, one could imagine a second *genus* of hydromagnetic waves, which dominate the wave flux and cause acceleration at distances of 10–20 $R_\odot$, but are sufficiently damped by 60 $R_\odot$ to leave little vestige in the *Helios* data. What is clearly necessary is information about the turbulence throughout the acceleration region.

IPS provides such information, as indicated in Figures 4 and 5. However, as mentioned in the introduction, a full retrieval of this information would require we understand the relationship between magnetic field spatial power spectra and density power spectra. Such knowledge at present does not exist, which limits the utility of IPS data. However, in the absence of such a full theory of compressible turbulence, we will make the simplest approximation that the density and magnetic field power spectra are proportional to each other. Our assumption is that the functional dependences on wavenumber and heliocentric distance of the two spectra are the same.

This extreme simplification has some support in solar wind observations. As stated repeatedly in this article, the density spectra on the spatial scales we are concerned with are well described by a Kolmogorov spectrum. The same is true of magnetic spectra for spatial wavenumbers above a spectral break which occurs on scales much larger than those which correspond to the density fluctuations probed by IPS (Bavassano et al. 1982; Marsch 1991; Roberts 1989). In addition, a recent study of solar wind density fluctuations (Klein et al. 1993), again utilizing *Helios* data, shows an excellent correlation between the magnitude of normalized density fluctuations and the "Mach number" of the turbulence. The Mach number for them is defined as $\delta v/C_s$ where δv is the turbulent velocity fluctuation and C_s is the sound speed. For Alfvénic turbulence $\delta b/B_0 = \delta v/V_A$, so the relationship reported by Klein et al. (1993) may also be stated as $\delta n/n_0 \simeq \beta^{-1/2}(\delta b/B_0)$, where β is the plasma beta, taken here as the square of the ratio of the sound speed to the Alfvén speed. This relationship gives a direct proportionality between the normalized density and magnetic field fluctuations, as we are assuming. It should be noted that Klein et al. (1993) find linear "Mach number" scaling only for regions of slow solar wind; for high-speed streams the scaling is more complicated and may be roughly consistent with pseudosound descriptions of compressible turbulence (Matthaeus et al. 1991). In the previous subsection we presented evidence that regions of slow solar wind dominate the radio wave scattering, so the use of empirical relations for the compressibility of turbulence in slow solar wind regions seems appropriate.

Equations (12) and (13) strictly describe the evolution of the square amplitude of a hydromagnetic wave in an inhomogeneous wind. We are interested in the spectral density in a broadband, power-law turbulence. The evolution of a broadband turbulence spectrum in the solar wind is considered by Tu, Pu, & Wei (1984) and Tu (1988). Tu and colleagues develop an expression for the evolution with heliocentric distance of the temporal power spectrum of magnetic field fluctuations $P_B(f)$ corresponding to $P_{\delta n}(f)$ described above. The evolution equation of Tu et al. (1984) and Tu (1988) includes terms for evolution in the inhomogeneous solar wind as well as nonlinear transfer of spectral energy. Tu obtains the remarkable result that for a Kolmogorov spectrum the radial evolution of $P_B(f)$ adheres to the WKB formula, equations (12) and (13). Given our assumptions about the correspondence between density and magnetic field fluctuations, we can then ask if the IPS-derived parameter C_N^2 adheres to equations (12) and (13).

The radial dependence of C_N^2 was measured by a least-squares fit of $C_N^2 \propto R^{-\kappa}$ to the data shown in Figure 5. All data points were used in the fit except the high-speed stream value of C_N^2, since it clearly deviates from the other measurements as discussed in § 4.1. The result of the fit is $\kappa = 3.72 \pm 0.30$. If we model the solar wind density profile as $\mu \equiv \rho/\rho_0 \propto R^{-\beta}$, and consider points far from the Alfvénic point so that $\mu \ll 1$, equation (12) predicts that $C_N^2 \propto R^{-3\beta/2}$. The simplest density profile to consider is the R^{-2} form of an asymptotic wind. If we use this model, we would predict that C_N^2 should be inversely proportional to the cube of the heliocentric distance. The actual dependence is steeper, indicating that there is stronger density turbulence close to the Sun than would be predicted by WKB evolution in a $\mu \propto R^{-2}$ wind. This is exactly the sort of signature one would look for as evidence of enhanced turbulence close to the Sun which might accelerate the solar wind.

The recent article of Bird et al. (1994) was therefore of particular interest to our analysis. Bird et al. (1994) used measurement of the dispersion measure of the *Ulysses* spacecraft beacon to measure the heliocentric distance dependence of μ over the range 4–40 $R_\odot$. What makes the work of Bird et al. (1994) particularly useful is that the measurements were made in 1991 August, exactly the epoch of our scattering measurements. Bird et al. (1994) parameterize their data in terms of κ and find a value of 2.54 for ingress and 2.42 for egress. Taking a rough mean of 2.50 for use in the above formulas, we find an expected dependence of C_N^2 on heliocentric distance as $R^{-3.75}$, in excellent agreement with the measurements in Figure 5.

Our view of the significance of Figure 5 may be stated as follows. The connection of the VLBI determinations of C_N^2 with those obtained from the *Helios* data indicates continuity of the turbulence and consistency of the measurement techniques. Subject to our assumption of the direct proportionality between density and magnetic turbulence spectra, which certainly merits more scrutiny and a more sophisticated treatment, the radial evolution of C_N^2 over the heliocentric distance interval 10–50 $R_\odot$ is in excellent agreement with the deductions of Roberts (1989). Our data show no indication of a departure from the WKB formula for turbulent evolution with heliocentric distance, nor the presence of a new *genus* of highly dissipative (and thus presumably compressive) turbulence in the inner solar wind.

Our data thus tend to support the implications discussed by Roberts (1989) for theories of turbulent heating and acceler-

ation of the solar wind, and promote alternative theories such as that of Scudder (1992). However, it is necessary to append an important qualification to this conclusion. The results of § 4.1 show that plasma in regions of slow-speed solar wind dominates the IPS measurements. These regions have flow speeds which are not greatly in excess of the speeds attainable with purely thermal models for the solar wind, so there is not a strong theoretical argument for wave-generated heating and acceleration. It is the high-speed streams which possess velocities substantially in excess of those attainable through thermally driven winds, and for which wave-assisted acceleration is required. Perversely, it appears that IPS is much less sensitive to these regions.

We nonetheless feel that our result is of interest and utility. An examination of Figure 2 of Roberts (1989) shows that adherence of the turbulent amplitude to the WKB formula over the range 1.0–0.3 AU is not dependent on stream structure. Roberts comments that variations in plasma quantities along a given flow tube apparently are more gradual, and describable by WKB theory, than are stream to stream variations. An expansive summary of Roberts's results would be that the same function of heliocentric distance describes evolution of turbulence in both high and low-speed streams. The conclusion to be drawn from Figure 5 is that the same function is compatible with the data all the way into 10 $R_\odot$, albeit with a measurement which is biased toward slow-speed solar wind.

Furthermore, if one posits that the genus of waves responsible for solar wind heating and acceleration is *totally* restricted to those regions of the corona which become the high-speed streams, they cannot enhance the value of C_N^2 in these regions by an amount ≥ 100 times the WKB value, or we would see greater scattering at 10 $R_\odot$. This may not seem to be a restrictive limit, but it can be noted that the waves seen in situ by *Helios* have very low damping rates, and most wave damping mechanisms which come to mind involve a substantial increase in the wave compressibility. If such compressive waves are present in the region of solar wind acceleration, they would enhance the radio scattering properties of that part of space. Future observations studies could explore this issue by making measurements which are sensitive to flow speeds in the turbulent plasma as well as C_N^2.

In addition to the aforementioned interpretational notes of caution, it is worth noting two reservations of an observational nature. Our support of the thesis of Roberts (1989) relies on the fit to the data in Figure 5. Obviously the point at 10 $R_\odot$, representing the observations of 0851+202 on 1991, August 3, is of paramount importance to this fit, and thus our interpretation. If our measurement were a substantial underestimate, the possibility of intense turbulence close to the Sun would again be viable. Although we believe this measurement is sound, it is worth noting two ways in which it might be an underestimate. First, the observations of 0851+202 on August 3 were made when the source was at a high heliographic latitude. As noted previously, Bourgois & Coles (1992) have found that at times of solar minimum the magnitude of the scattering over the Sun's poles is much less than in the ecliptic plane. Such an effect would be exactly of the form, in principle, to cause us to underestimate the scattering close to the Sun. We do not believe this is a problem here, since the corona was not in a solar minimum configuration at the time of the observations. However, it would be desirable to have future observations throughout the solar cycle, and at a range of heliographic latitudes on the same observing day.

The second possibility is that some bias affects measurements of the phase scintillation variance, and thus D_ϕ at times when the phase scintillations are particularly strong. An example of such a process would be a bias due to "bad calls" in the reconstituted phase time series as discussed in § 2.3. A concern of precisely this sort is what motivated the simulation studies of the reconstitution process described there. However, as noted in § 2.3, the simulation exercises seemed rather to indicate that the D_ϕ measurements were relatively immune to the effect of phase jumps. Nonetheless, future work, comprising both new observations as well as further time series analyses of the phase folding and reconstitution process, would be desirable and reassuring.

5. SUMMARY AND CONCLUSIONS

The results of this study of VLBI phase scintillations may be summarized as follows.

1. The phase structure function D_ϕ on baselines of 200–2000 km was measured at four solar elongations ranging from 10 to 50 $R_\odot$, using 5.0 and 8.4 GHz VLBI phase scintillations. A number of techniques for measuring σ_ϕ^2 and thus D_ϕ were discussed and examples given.
2. Our measurements of D_ϕ are in quite good agreement with the form of the phase structure function published by Coles & Harmon (1989), which is largely deduced from measurements on different spatial scales than ours.
3. Our observations show that a Kolmogorov spectrum is a good representation of the density power spectra on spatial scales of 200–2000 km.
4. The scattering at 10 $R_\odot$ appears to be anisotropic, with an axial ratio $\simeq 2.0 \pm 0.5$. The data are consistent with magnetic field-aligned irregularities in the outer corona. The degree of anisotropy may be slightly less than previously reported for measurements on shorter baselines by Armstrong et al. (1990).
5. The values of the density spectrum normalization constant obtained from our IPS measurements at solar elongations of 40–50 $R_\odot$ are in acceptable agreement with the values inferred from *Helios* spacecraft in situ measurements at perihelion, $\simeq 70$ $R_\odot$. However, the IPS measurements are comparable to *Helios* C_N^2 measurements made in slow solar wind. The high-speed streams sampled by *Helios* do not have sufficiently intense density turbulence to account for the IPS observations.
6. The heliocentric distance dependence of C_N^2 is consistent with WKB evolution of the turbulence between $\simeq 10$ $R_\odot$ and $\simeq 70$ $R_\odot$. This result is consistent with the analysis of Roberts (1989), and supports the conclusion that there is insufficient MHD wave flux close to the Sun to drive the solar wind. This conclusion, however, is tempered by the realization that our measurements are probably dominated by the slow-speed solar wind, whereas it is the high-speed wind for which there is the greatest need for wave acceleration.

The authors thank Robert Mutel for several important discussions on interferometer phase scintillations. Britt Scharringhausen assisted in data analysis. This work was supported at the University of Iowa by grant ATM 92-16821 from the National Science Foundation, and grant NAGW-1594 from NASA. The Very Long Baseline Array of the National Radio Astronomy Observatory is operated by Associated Universities, Inc., under contract from the National Science Foundation. We gratefully acknowledge the thorough review of this

paper by the referee, William Coles, as well his helpful suggestions and discussions. We also thank him for use of his unpublished measurements of the solar wind velocity at the time of our observations. English translations of the praecepts of Heraclitus of Ephesus are due to C. H. Kahn, The Art and Thought of Heraclitus, Cambridge University Press.

REFERENCES

Ananthakrishnan, S., Coles, W. A., & Kaufman, J. J. 1980, J. Geophys. Res., 85, 6025
Armstrong, J. W., Coles, W. A., Kojima, K., & Rickett, B. J. 1990, ApJ, 358, 685
Bavassano, B., Dobrowolny, M., Mariani, F., & Ness, N. F. 1982, J. Geophys. Res., 87, 3617
Bevington, P. R. 1969, Data Reduction and Error Analysis for the Physical Sciences (New York: McGraw-Hill)
Bird, M. K., Volland, H., Patzold, M., Edenhofer, P., Asmar, S. W., & Brenkle, J. P. 1994, ApJ, 426, 373
Blesing, R. G., & Dennison, P. A. 1972, Proc. Astron. Soc. Australia, 2, 84
Bourgois, G. 1993, in Spatio-Temporal Analysis for Resolving Plasma Turbulence (ESA Publ. WPP-047), 157
Bourgois, G., & Coles, W. A. 1992, in Solar Wind Seven, ed. E. Marsch & R. Schwenn (Oxford: Pergamon), 155
Coles, W. A. 1978, Space Sci. Rev., 21, 411
Coles, W. A., Esser, R., Lovhaug, U. P., & Markkanen, J. 1991b, J. Geophys. Res., 96, 13849
Coles, W. A., & Harmon, J. K. 1989, ApJ, 337, 1023
Coles, W. A., Liu, W., Harmon, J. K., & Martin, C. L. 1991a, J. Geophys. Res., 96, 1745
Cordes, J. M., Weisberg, J. M., & Boriakoff, V. 1985, ApJ, 288, 221
Esser, R., Leer, E., Habbal, S. R., & Withbroe, G. L. 1986, J. Geophys. Res., 91, 2950
Hewish, A. 1958, MNRAS, 118, 534
Hollweg, J. V. 1992, in Solar Wind Seven, ed. E. Marsch & R. Schwenn (Oxford: Pergamon), 53
Klein, L., Bruno, R., Bavassano, B., & Rosenbauer, H. 1993, J. Geophys. Res., 98, 7837
Kojima, M., Washimi, H., Misawa, H., & Hakamada, K. 1992, in Solar Wind Seven, ed. E. Marsch & R. Schwenn (Oxford: Pergamon), 201
Marsch, E. 1991, in Physics of the Inner Heliosphere, ed. R. Schwenn & E. Marsch (Berlin: Springer-Verlag)
Marsch, E., & Tu, C. Y. 1990, J. Geophys. Res., 95, 11945
Matthaeus, W. H., Klein, L. W., Ghosh, S., & Brown, M. R. 1991, J. Geophys, Res., 96, 5421
Montgomery, D., Brown, M. R., & Matthaeus, W. H. 1987, J. Geophys. Res., 92, 282
Montgomery, D., & Turner, L. 1981, Phys. Fluids, 24, 825
Mutel, R. L. 1975, Ph.D. thesis, Univ. Colorado
Narayan, R., Anantharamaiah, K. R., & Cornwell, T. J. 1989, MNRAS, 424, 142
Rickett, B. J., & Coles, W. A. 1991, J. Geophys. Res., 96, 1717
Roberts, D. A. 1989, J. Geophys. Res., 94, 6899
Sakurai, T. 1993, Ph.D. thesis, Univ. Iowa
Sakurai, T., Spangler, S. R., & Armstrong, J. W. 1992, J. Geophys. Res., 97, 17141
Scudder, J. D. 1992, ApJ, 398, 319
Tu, C. Y. 1988, J. Geophys. Res., 93, 7
Tu, C. Y., Pu, Z. Y., & Wei, F. S. 1984, J. Geophys. Res., 89, 9695
Woo, R., & Armstrong, J. W. 1979, J. Geophys. Res., 84, 4288
Woo, R., & Gazis, P. 1993, Nature, 366, 543
Zank, G. P., & Matthaeus, W. H. 1992, J. Plasma Phys., 48, 85